Universiteit Utrecht

Opleiding Natuur- en Sterrenkunde

Towards absolute scattering cross section of nanoparticles and single molecules

Bachelor Thesis

Zeyu Kuang

Supervisors:

Dr. Siddharth Ghosh
Debye Institute for Nanomaterials Science

Dr. Sanli Faez
Debye Institute for Nanomaterials Science

May 26,2017

Abstract

Elastic scattering signal from optically active molecules below the Rayleigh regime can be detected by probing its absorption band. Within the absorption band, the optical scattering cross section (SCS) of the molecule is a rapidly varying function of light frequency. Knowing the absolute SCS of a single molecule has many applications like learning about the internal molecular levels (orbitals), or identifying molecules or some chemical processes. For this reason, we proposed an experimental scheme for measuring the absolute SCS of nanoparticles and single molecules. We developed a setup for this measurement, from where, currently, we obtained relative SCSs of particles with low extinction. Further improving the setup and samples will lead us towards absolute SCSs of small particles (like single fluorophores) and quantitative description of resonance light scattering.

Acknowledgment

I am sincerely grateful to Dr. Siddharth Ghosh for supervising me during this semester. You are like a friend and a father to me, always encouraging, disciplining, but never neglecting me. This thesis would not have been possible without your tremendous support. It has been a real honor to work with you while enjoying the pleasure of pursuing scientific truth. From you, I learned how to become a true physicist.

A special thanks to Dr. Sanli Feaz for his supervision and expert advice throughout this difficult project. Your candor and humor motivated me across the whole process and thank you for offering your precious time and patience.

My gratitude also goes to other members in LINX group - Allard, Pritam, Jeroen, Abhilash, Dashdeleg, Xiaoqing, and Bohdan. Your care and support made me feel like I was working with a family and the orange tones at every Tuesday meeting is now a memory of home!

I am grateful to all three technicians - Dante, Cees, Paul, and secretary Mijke for their kind and generous help during my experiment.

I would also like to thank Javier and other members in the Debye institute, for your warm companionship during my stay in Utrecht.

I am in appreciation of Kegel group for the provision of CPSAA particles.

I would like to thank my best roommates - Liting, Renee, and Alejandro. Your company has made staying in Utrecht colorful and memorable. I also thank all my friends in China, Lidan, Qian, Lu, Bowen, Ruizhe, and Zexun, for all your help and encouragement despite our distance.

And finally, last but by no means least, I want to thank my parents who have supported and continue to support me all the time. Your love is the most precious gift I could ever deserve.

Contents

1 Introduction

How do we see any objects in our daily life? Lights from the sun incidents on the objects and the scattered light from the object gets detected in our eyes by certain photosensitive receptors. Light scattering governs optical phenomena like reflection and refraction. The analysis of the scattered light can reveal information about the structure of a material. There are two kinds of scattering processes: elastic scattering and inelastic scattering [1]. In elastic scattering, the wavelength of the light remains the same during the scattering process, while in inelastic scattering, it changes. In elastic scattering, if the wavelength of the incident light is much larger than the size of the particle, then this scattering process is called Rayleigh scattering [2]. For a certain wavelength, the intensity of the Rayleigh scattering is proportional to the sixth power of the size of the particle [3]. Elastic scattering signal will drop as the size of the particle decreases. Normally, when the size of the particle is below nanometer scale, the elastic scattering signal of a single particle is no longer recognizable from other molecules in the environment. However, using inelastic scattering, one can separate molecules by their specific frequency response. Thus, for single molecules detection, people often use inelastic scattering, such as fluorescence spectroscopy [4–6] and Raman scattering [7–9], rather than elastic scattering.

Motivation

Two decades ago, a technique was proposed by Robert F.Pasternack and Peter J.Collings[10], called resonance light scattering (RLS), from where elastic scattering was used for measuring aggregation and identifying certain proteins. This technique has the potential to perform high resolution spectroscopy in contrast to state of the art fluorescence spectroscopy [11] because elastic scattering does not suffer from bleaching [12–14] or blinking [15–17]. Although many works have been done in this area [18–22], none of them has measured RLS quantitatively. This motivates us to develop an experimental setup for measuring the absolute SCS of nanoparticles and single molecules. In the future, this can be used to measure the absolute SCS of the fluorophores, which will give a quantitative description on the RLS.

Summary

In this thesis we presented a scheme for measuring the absolute SCS of nanoparticles and single molecules. Based on the scheme, we developed a setup to demonstrate relative SCSs of particles with low extinction. We tested the setup by measuring the relative SCSs of gold nanoparticles (Au NPs), whose theoretical SCSs were also calculated using Mie theory. We found a good agreement between experimental and theoretical relative SCSs of Au NPs. This confirmed the reliability of our setup. Furthermore, we used this setup in two applications:

1. We measured the relative SCSs of pH-sensitive particles (negatively charged Polyacrylic acid-decorated small polystyrene nanospheres or CPSAA) under different pH. CPSAA's size is dependent on pH. We analysed sizes at different pH by analysing the change of SCS of CPSAA.

2. We measured RLS of fluorescent dye molecules.

Outline

The remainder of the thesis is organized as follows. In chapter 2, section 2.1 gives an overview of Mie theory and corresponding methods to simulate the SCS of nanoparticles. Section 2.2 describes the scheme we used for measuring the SCS of nanoparticles and single molecules. Section 2.3 presents our experimental setup. This setup was also tested by gold nanoparticles using the scheme described in section 2.2. In section 2.4, we demonstrate how our method was put into practice by measuring the size of CPSAA, as well as the RLS of fluorophores. In chapter 3, we conclude the thesis by discussing the main findings and future improvements on the setup.

2 Methods

In this chapter, we present a setup and methods for measuring the SCS of nanoparticles and single molecules, as well as a way to simulate it using Mie theory. We demonstrated the validity of our measurement by comparing relative SCSs of Au NPs from both simulation and experiment. Additionally, we made two observations using our the setup. Firstly, we observed the size change of the pH-sensitive particles. Secondly, we measured RLS of fluorophores and observed their elastic scattering signal.

2.1 Mie theory and simulation

We measured SCSs of various nanoparticles with the concentration at single particle level. We simulated the SCS of a nanoparticle using Mie theory [23]. In the simulation, we consider the geometric shape of the nanoparticle as a sphere. The Mie theory calculates the scattering field from the Maxwell's equations of a sphere with homogeneous refractive index in the absence of surface charges or currents. The key parameters in the Mie theory are the Mie coefficients (a_n, b_n, c_n, and d_n), where a_n and b_n account for the scattering field and c_n and d_n account for the internal field.

We focus primarily on a_n and b_n because we need to obtain the scattering field for calculating SCS [24]:

$$a_n = \frac{m^2 j_n(mx)[xj_n(x)]' - j_n(x)[mxj_n(mx)]'}{m^2 j_n(mx)[xh_n^{(1)}(x)]' - h_n^{(1)}(x)[mxj_n(mx)]'} \tag{1}$$

$$b_n = \frac{j_n(mx)[xj_n(x)]' - j_n(x)[mxj_n(mx)]'}{j_n(mx)[xh_n^{(1)}(x)]' - h_n^{(1)}(x)[mxj_n(mx)]'} \tag{2}$$

where m is the refractive index of the sphere relative to the surrounding medium, $x = ka$ is the size parameter, a is the radius of the sphere, $k(= 2\pi/\lambda)$ is the wave number, and λ is the wavelength in the surrounding medium, with relative permeability equals to 1. The functions $j_n(z)$ and $h_n^{(1)}(z) = j_n(z) + iy_n(z)$ are spherical Bessel functions. Scattering cross section, σ_{sca}, is defined as:

$$\sigma_{sca} = \frac{W_{sca}}{I_{inc}} \tag{3}$$

where I_{inc} represents the intensity incident on the surface of the particle and W_{sca} is the scattered energy. The relation among σ_{sca}, a_n, and b_n is:

$$\sigma_{sca} = \frac{2\pi}{k^2} \sum_{n=1}^{n_{max}} (2n+1)(|a_n|^2 + |b_n|^2). \tag{4}$$

All the infinite series can be truncated after n_{max} terms [23], which is determined by x:

$$n_{max} = x + 4x^{\frac{1}{3}} + 2 \tag{5}$$

Using the equation (4), we calculated σ_{sca} of Au NPs for different diameters (d) as shown in Figure 1, where water is the surrounding medium. This result agrees with the others [26].

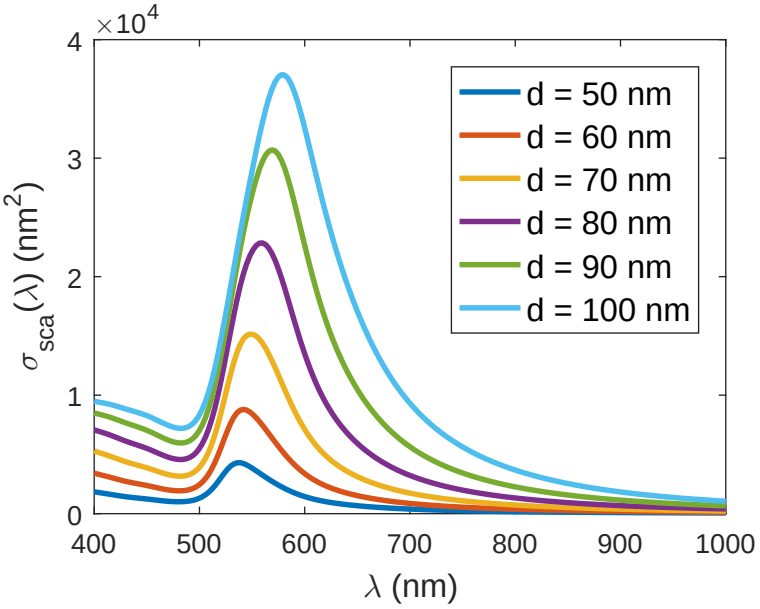

Figure 1: Simulated $\sigma_{sca}(\lambda)$ of Au NPs for different diameters (d), using Mie theory. Surrounding medium is water with refractive index 1.33. The refractive index of Au is from Johnson and Christy [25]. As the diameter of Au NPs changes from 50 nm to 100 nm, $\sigma_{sca}(\lambda)$ increases from 4.3×10^7 nm^2 to 3.7×10^8 nm^2, the resonacne peak shifts from 536 nm to 578 nm.

2.2 Experimental schemes

In this section, we proposed experimental schemes for measuring the absolute SCS of small particles. Afterwards we simplified the scheme for particles with low extinction. In the end, we further modify it to measure only the relative SCS.

Setup illustration: As shown in Figure 2, placed in the center is the particle solution with low concentration to avoid aggregation effect. Light from incident channel illuminates the particles with incident power[1], $P_{in}(\lambda)$. Scattering channel records part of scattered power, $P_{out}(\lambda)$, while transmission channel records the transmitted power, $P_t(\lambda)$. More than one particle is presented in the intersection between the detection and illumination area. However, as long as the particle concentration, C_p, is low enough that there's no aggregation effect, we can obtain the SCS of a single particle by dividing the scattering signal by the number of particles after proper geometrical considerations.

2.2.1 Absolute scattering cross section

(a) Measurement scheme for small particles: For small particles, the ratio between $P_{out}(\lambda)$ and $P_t(\lambda)$ is proportional to C_p added by background, $b_p(\lambda)$:

$$\frac{P_{out}(\lambda)}{P_t(\lambda)} = k_p(\lambda)C_p + b_p(\lambda) \tag{6}$$

with $k_p(\lambda)$ proportional to $\sigma^p_{sca}(\lambda)$ with the coefficient, $A(\lambda)$, caused by the instrument[2]:

$$k_p(\lambda) = A(\lambda)\sigma^p_{sca}(\lambda). \tag{7}$$

[1] In reality, we used lenses to focus the incident light.

[2] Equation (6) and (7) are derived in Appendix A

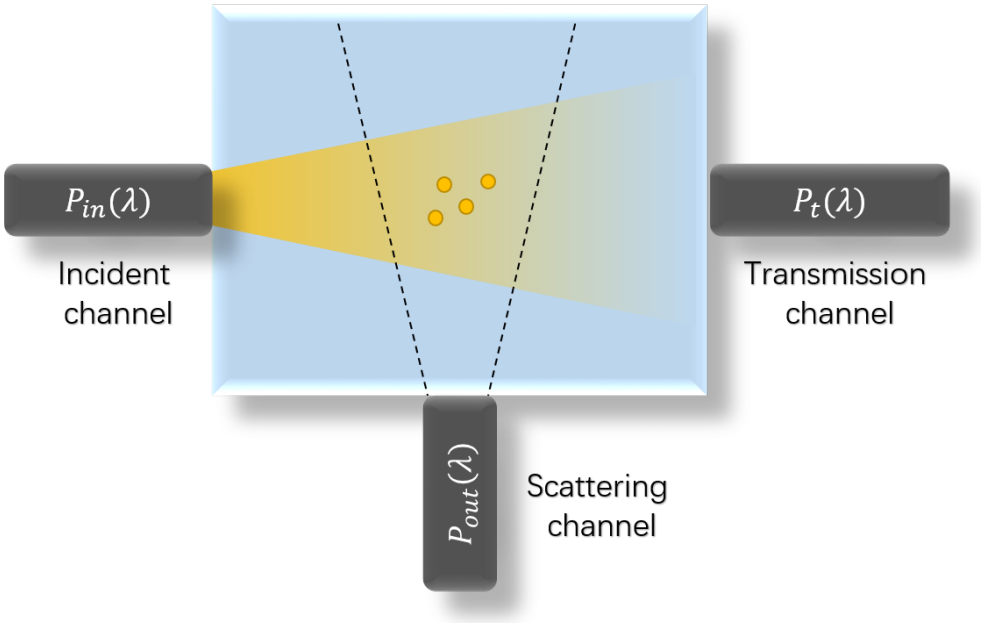

Figure 2: **Setup illustration:** In our scheme, particles inside the solution are illuminated by the incident light with power $P_{in}(\lambda)$. Scattering channel collects part of the scattered power, $P_{out}(\lambda)$, while the transmission channel records the transmitted power, $P_t(\lambda)$.

Based on equation (6), we measure $P_{out}(\lambda)$ and $P_t(\lambda)$ for different C_p to get the linear dependency, $k_p(\lambda)$. Once we obtain $k_p(\lambda)$ from the measurement, we are able to calculate $\sigma^p_{sca}(\lambda)$ as long as we know $A(\lambda)$. In order to know $A(\lambda)$, a reference with known SCS, $\sigma^r_{sca}(\lambda)$, is measured using the same setup. We recorded $P_{out}(\lambda)$ and $P_t(\lambda)$ for the reference with different concentration, C_r, to obtain their linear dependency, $k_r(\lambda)$:

$$\frac{P_{out}(\lambda)}{P_t(\lambda)} = k_r(\lambda)C_r + b_r(\lambda) \tag{8}$$

The relation between $k_r(\lambda)$ and $\sigma^r_{sca}(\lambda)$ is:

$$k_r(\lambda) = A(\lambda)\sigma^r_{sca}(\lambda) \tag{9}$$

Combining equations (8) and (9), $\sigma^p_{sca}(\lambda)$ is:

$$\sigma^p_{sca}(\lambda) = \frac{k_p(\lambda)}{k_r(\lambda)}\sigma^r_{sca}(\lambda). \tag{10}$$

(b) Measurement scheme for particles with low extinction: In general cases, both the scattering and the transmission signal need to be monitored. However, for particles with low extinction, only the scattering signal is necessary for determining the absolute SCS.

If we assume $P_{in}(\lambda)$ stays constant, then $P_{out}(\lambda)$ is proportional to C_p:

$$P_{out}(\lambda) = k_p(\lambda)C_p + b_p(\lambda) \tag{11}$$

with a new $k_p(\lambda)$ defined as:

$$k_p(\lambda) = A(\lambda)P_{in}(\lambda)\sigma^p_{sca}(\lambda). \tag{12}$$

A reference is tested under the same setup, which gives us

$$k_r(\lambda) = A(\lambda)P_{in}(\lambda)\sigma^r_{sca}(\lambda). \tag{13}$$

Combining equations (12) and (13), we get

$$\sigma^p_{sca}(\lambda) = \frac{k_p(\lambda)}{k_r(\lambda)}\sigma^r_{sca}(\lambda). \tag{14}$$

Equation (14) looks the same as equation (10), but their $k_p(\lambda)$ and $k_r(\lambda)$ are defined differently, which only requires measuring scattering signal, $P_{out}(\lambda)$.

2.2.2 Relative scattering cross section

It is always a challenge to know the absolute concentration of the particle. Without the knowledge of the absolute concentration, what we calculate could only be relative SCS. Nonetheless, the relative SCS still contains useful information and worth investigating.

In the relative SCS measurement[3], instead of the absolute concentration, C_p, we use relative concentration, $C_{p(rel)}$, to calculate $k_p(\lambda)$:

$$P_{out}(\lambda) = k_p(\lambda)C_{p(rel)} + b_p(\lambda) \tag{15}$$

$$k_p(\lambda) = A(\lambda)P_{in}(\lambda)\sigma^{p(rel)}_{sca}(\lambda). \tag{16}$$

For the reference whose relative concentration is $C_{r(rel)}$, we have

$$P_{out}(\lambda) = k_r(\lambda)C_{r(rel)} + b_p(\lambda) \tag{17}$$

$$k_r(\lambda) = A(\lambda)P_{in}(\lambda)\sigma^r_{sca}(\lambda). \tag{18}$$

Combining equations (16) and (18), we get

$$\sigma^{p(rel)}_{sca}(\lambda) = \frac{k_p(\lambda)}{k_r(\lambda)}\sigma^r_{sca}(\lambda). \tag{19}$$

In this case, $k_p(\lambda)$ is also relative since it is defined by the relative concentration, $C_{p(rel)}$, same as $k_r(\lambda)$.

2.3 Experimental setup

We brought up several experimental schemes on measuring the SCS of nanoparticles and single molecules. In this section, we present our setup and test its reliability. In the reliability test, we implemented the 'relative scattering cross section measurement' scheme on Au NPs of different sizes. We used one size as a reference to calculate the relative SCSs of others. We also simulated their theoretical SCSs. We compared the theoretical SCSs with the experimental SCSs to get the reliability of our setup.

[3]This scheme follows the 'Measurement scheme for particles with low extinction'. One can easily draw an analogy for measuring the relative SCS of particles with high extinction.

2.3.1 Setup

The setup diagram is shown in Figure 3. We used a super continuum laser source [27] to produce a broadband laser light. We coupled the light into our monochromator by an optical fiber. We built our monochromator in a way that it has two modes: broadband mode and monochromatic mode[4]. We coupled the light coming out of the monochromator into fiber 1, then focused the light to the entry of the fiber 3 through several lenses inside the focusing part. Along its way inside the cuvette, light was scattered by the particle solution. A portion of the scattered light was collected by fiber 2 and received in the spectrometer 1. Most of the transmitted light was collected by the fiber 3 after being attenuated by a diffuser. In the end of the fiber 3, spectrometer 2 collected the attenuated transmitted light.

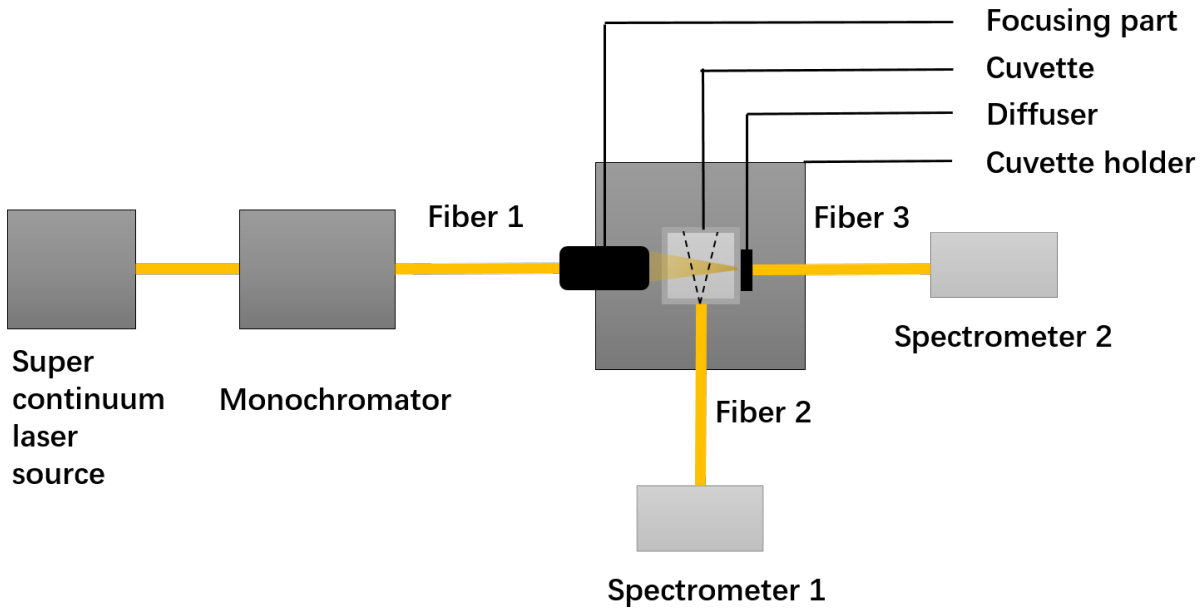

Figure 3: Setup diagram for measuring the SCS for nanoparticles and single molecules. Setup has five major parts - Laser source, monochromator, cuvette holder, spectrometer 1, and spectrometer 2[5]. Cuvette, diffuser, focusing part, fiber 1, fiber 2, and fiber 3 are integrated in the cuvette holder.

2.3.2 Reference measurement

In 'relative scattering cross section' measurement scheme, a reference with known SCS was measured in order to obtain information about the instrument response, which was used to calculate SCSs of the other particles. This reference measurement is important because any error within the reference will effect the analysis of other measurements. So before measuring the SCS of any other particle, a measurement on the reference needed to be conducted.

[4]Broadband mode allows the broadband light pass through the monochromator. This mode is used for measuring non-fluorescent particles. Monochromatic mode selects one wavelength in the broadband light. This mode is used for measuring fluorescent particles.

[5]See the appendix B for further information on the setup.

(a) Instrument response function: Every instrument will have a certain amount of effect on the original signal, either attenuate its intensity or shift its frequency. In order to extract the original signal, we need to measure instrument response function, $IRF(\lambda)$, which is the ratio between the obtained signal and the original signal from a standard reference [28].

In our case, obtained signal, $P_{out}(\lambda)$, is proportional to $k_r(\lambda)$. Original signal is proportional to $\sigma^r_{sca}(\lambda)$. We define $IRF(\lambda)$ as:

$$IRF(\lambda) = \frac{k_r(\lambda)}{\sigma^r_{sca}(\lambda)}. \tag{20}$$

Combining equations (19) and (20), we can obtain $\sigma^{p(rel)}_{sca}(\lambda)$:

$$\sigma^{p(rel)}_{sca}(\lambda) = \frac{k_p(\lambda)}{IRF(\lambda)}. \tag{21}$$

Thus, we separate our measurements into two parts:

1. Measure the scattering signal of the reference to obtain $k_r(\lambda)$, and divide it by its theoretical SCS, $\sigma^r_{sca}(\lambda)$, to obtain $IRF(\lambda)$.

2. Measure the scattering signal of the particle of interest to obtain $k_p(\lambda)$, and apply $IRF(\lambda)$ to obtain $\sigma^{p(rel)}_{sca}(\lambda)$.

(b) Reference - 30 nm diameter of gold nanoparticles: We choose the 30 nm diameter of Au NPs (30 nm Au NPs) to be our reference. It is chosen because we can calculate its theoretical SCS, as we discussed in section 2.1. The theoretical SCS ,$\sigma^r_{sca}(\lambda)$, of a 30 nm Au NP is shown in Figure 4.

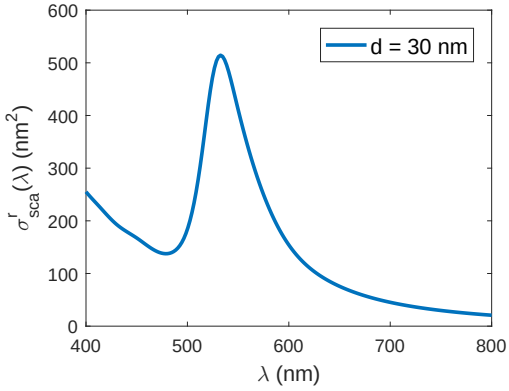

Figure 4: Theoretical SCS, $\sigma^r_{sca}(\lambda)$, for a Au NP with d = 30 nm. $\sigma^r_{sca}(\lambda)$ is calculated using Mie theory.

Since 30 nm Au NPs have low extinction, we followed the 'relative scattering cross section' measurement scheme[6]. As proved in this scheme, if we assume that the input power stays the same[7], we only need to measure the scattering signal.

In the measurement, we prepared a dilution series of 30 nm Au NPs. For the one with certain relative concentration, $C_{r(rel)}$, we measured its scattering signal, $P_{out}(\lambda)$. Based on equation (17), we extracted the linear coefficient, $k_r(\lambda)$, between $P_{out}(\lambda)$ and $C_{r(rel)}$ for each λ. $C_{r(rel)}$ changes from 1×, 10× to 10000×[8]. $P_{out}(\lambda)$ for all these different $C_{r(rel)}$ were shown in Figure 5(a).

[6]We only measured the relative SCS because we did not know the absolute concentration of 30 nm Au NPs.

[7]This assumption was being verified in the section 2.3.4.

[8]1× is the lowest relative concentration in the dilution series. N× has the concentration N times of the lowest one.

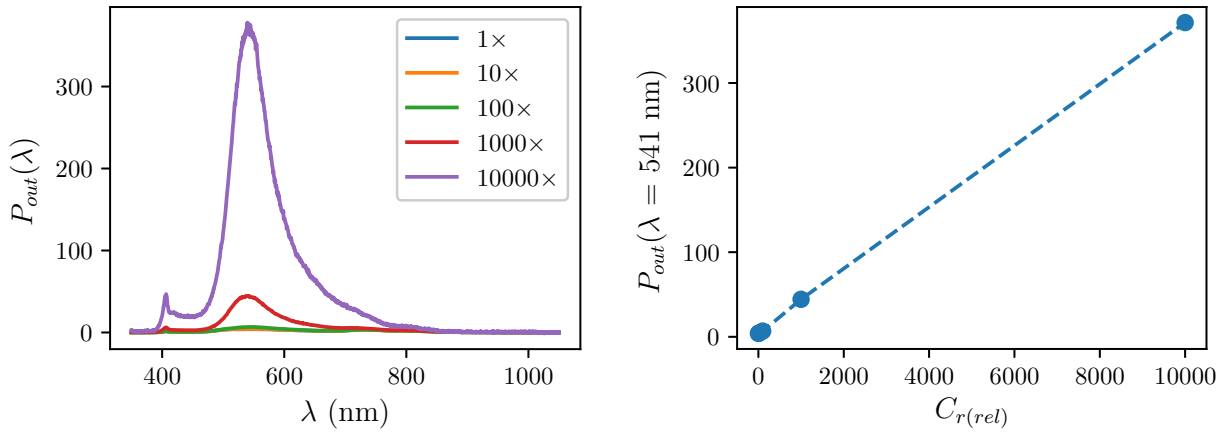

(a) (b)

Figure 5: **Scattering signal of 30 nm Au NPs dilution series:** The units of $P_{out}(\lambda)$ on both vertical axises are Relative Counts / ms. (a) $P_{out}(\lambda)$ of 30 nm Au NPs for different $C_{r(rel)}$ (b) P_{out} of 30 nm Au NPs as a function of $C_{r(rel)}$ at $\lambda = 541$ nm.

As we can see in Figure 5(a), $P_{out}(\lambda)$ decreases approximately 10 times after each 10 times dilution. The linear relation between $P_{out}(\lambda)$ and $C_{r(rel)}$ in Figure 5(b) shows that the 30 nm Au NPs are not aggregating and we are in the single particle concentration[9]. $k_r(\lambda)$ is calculated by fitting a linear function to $P_{out}(\lambda)$ and $C_{r(rel)}$ for each λ.

(c) Obtaining instrument response function: We obtained the $IRF(\lambda)$ from equation (20). The result is shown in Figure 6.

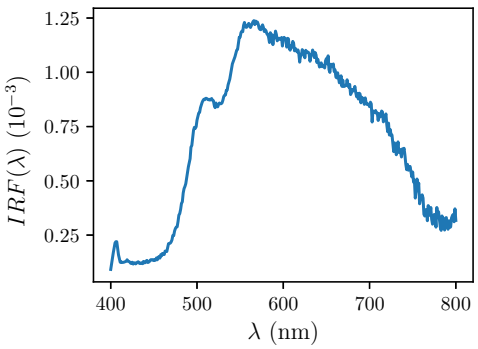

Figure 6: $IRF(\lambda)$ of the setup. The unit of $IRF(\lambda)$ on the vertical axis is Relative counts / (ms · nm^2).

Based on equations (18) and (20), $IRF(\lambda)$ is:

$$IRF(\lambda) = A(\lambda)P_{in}(\lambda). \tag{22}$$

The wavelength dependence of $P_{in}(\lambda)$ is encoded in the $IRF(\lambda)$.

2.3.3 Reliability measurements

We obtained $IRF(\lambda)$ from the scattering signal of the reference (30 nm Au NPs). In this section, we measured the scattering signal of 10 nm, 40 nm, and 100 nm Au NPs, and then applied $IRF(\lambda)$ to calculate their relative SCSs. In comparison with the experimental SCSs, we also calculated their theoretical SCSs using Mie theory mentioned in section 2.1.

Among all the samples, 100 nm Au NPs were taken as an example to illustrate the process of measurements and the data analyzing: We first

[9]This only confirms the linearity on $\lambda = 541$ nm, a more sufficient validation of the linearity over all range of λ is present on section 2.3.4.

prepared a dilution series of 100 nm Au NPs. For each concentration, we measured scattering signal, then applied $IRF(\lambda)$ calculated in section 2.3.2 to obtain the SCS of 100 nm Au NPs. In the end, we compared this result with the theory to get the reliability of our setup.

(a) Obtaining the relative SCS of 100nm Au NPs: We measured $P_{out}(\lambda)$ of the dilution series of 100 nm Au NPs, as shown in Figure 7(a). For the one with certain relative concentration, $C_{p(rel)}$, $P_{out}(\lambda)$ is given by the equation (15). We obtained $k_p(\lambda)$ in the same method described in section 2.3.2. The relative SCS of 100 nm Au NPs, $\sigma_{sca}^{p(rel)}(\lambda)$, was given by equation (21). The result is shown in Figure 7(b).

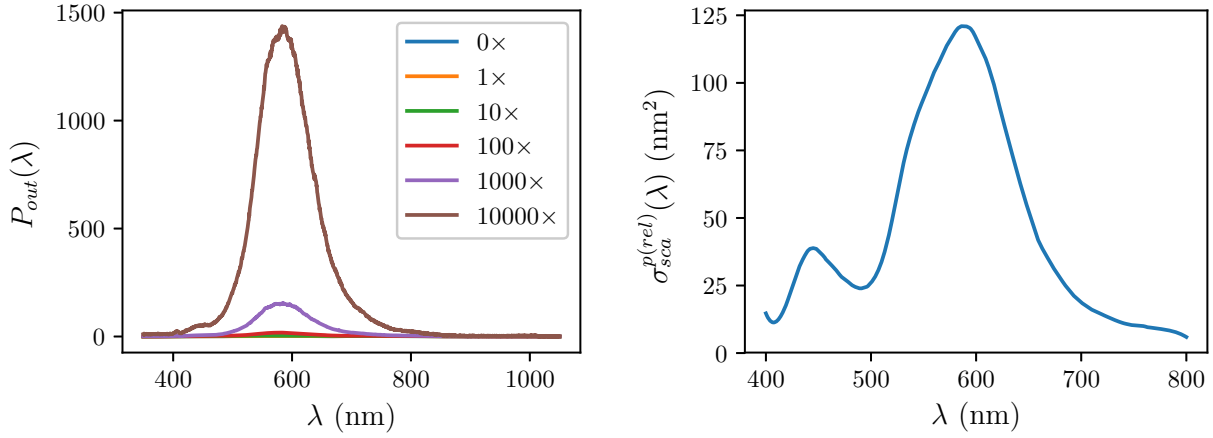

(a) (b)

Figure 7: (a) $P_{out}(\lambda)$ of 100 nm Au NPs for different $C_{p(rel)}$. The unit of $P_{out}(\lambda)$ is Relative Counts / ms. 0× is the contrast group (0 nM of Au NPs). (b) Experimental $\sigma_{sca}^{p(rel)}$ of 100 nm Au NPs, obtained using 30 nm Au NPs as the reference.

(b) Comparison with the theory: Apart from 100 nm Au NPs, $\sigma_{sca}^{p(rel)}$ of 10 and 40 nm were also measured where 30 nm Au NPs was considered as a reference. We normalized these $\sigma_{sca}^{p(rel)}$ over their peak values, as well as their theoretical counterparts. The result is shown in Figure 8.

By comparing the experimental and theoretical SCSs, we see that the surface plasmon resonance[10] of Au NPs is captured in our measurement. For 10 nm and 40 nm Au NPs, the resonance peak positions are the same as the theory. There are broadening around their peak shoulders and abnormalities from 400 to 450 nm. The peak position of the SCS of 100 nm Au NPs is red shifted 14 nm compared to the theory. These mismatch is due to the size distribution of the Au NPs.

Our reliability test shows that our setup is capable of measuring relative SCSs of nanoparticles. In order to measure their absolute SCSs and improve the precision, two more measurements are required:

[10]Surface plasmon resonance is a collective resonant oscillation of the free electrons of the conduction band of the metal[29, 30].

1. measure the absolute concentration of Au NPs to obtain its absolute SCS.
2. measure the size distribution of Au NPs and take it into account when calculating its theoretical SCS.

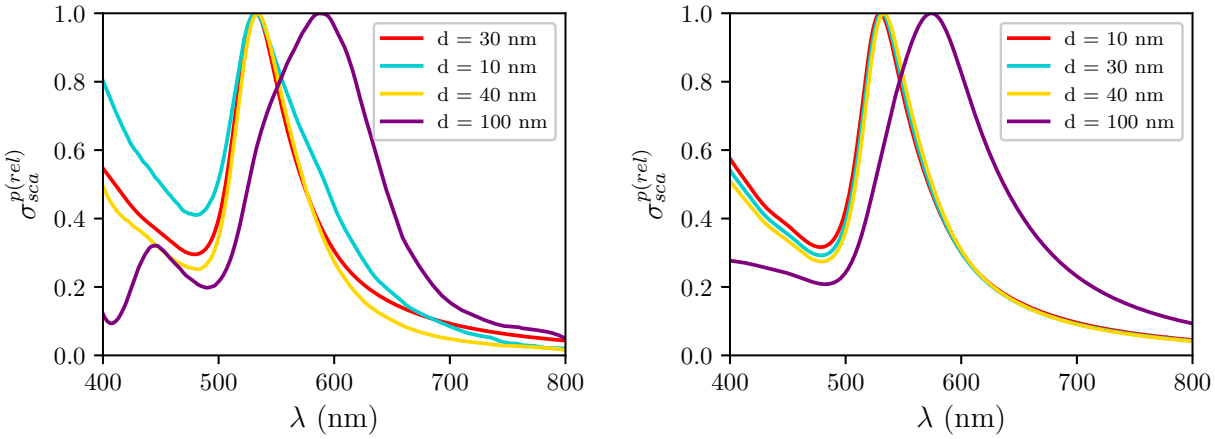

(a) (b)

Figure 8: **Normalized SCS for different diameters of Au NPs:** (a) Experimental $\sigma_{sca}^{p(rel)}$ calculated using 30 nm Au NPs as a reference. Experimental $\sigma_{sca}^{p(rel)}$ of 30 nm Au NPs is the same as the theory. This is because 30 nm Au NPs are used as the reference. (b) Theoretical $\sigma_{sca}^{p(rel)}$ simulated using Mie theory.

2.3.4 Uncertainties

Though the general shape of $\sigma_{sca}^{p(rel)}$ of 10 nm Au, 40 nm Au, and 100 nm Au are captured, there are still several artifacts: broadening of the peak, abnormality from 400 to 450 nm, and the red shift of the resonance of 100 nm Au NPs. All these disagreements between experiment and theory are largely due to the size variation in our gold samples, which we shall discuss in this part, as well as other uncertainties.

(a) Size variance of Au NPs: In our theoretical calculation, we didn't consider size distribution of Au NPs. This is the dominant cause responding for the disagreement between experiment and theory. As we can see in Figure 9, in 100 nm Au NPs solution, most particle diameter are around 110 nm. This causes the red shift of its relative SCS. Additionally, the large span of the size distribution leads to the broadening of our resonance peak. Likewise, in reference measurement we calculated the SCS of the reference (30 nm Au NPs) without considering its size distribution.

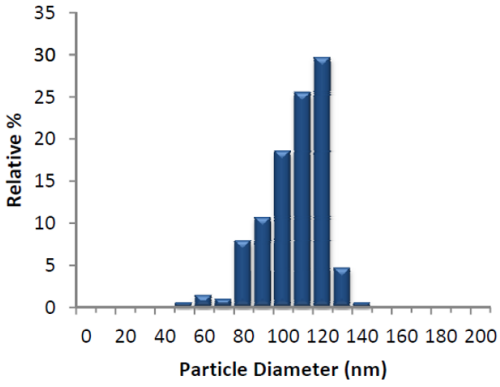

Figure 9: Size distribution of 100 nm Au. Diameter: 101.5 ± 15.1 nm[11].

[11]From datasheet of 100 nm PVP Gold provided by the company *nano Composix*.

This causes error in $IRF(\lambda)$ and will effect all other measurements. Hopefully, this problem can be solved by taking the size distribution into account when calculating the theoretical value, for both tested samples and the reference.

(b) Polarization effect: There should be a certain degree of polarization in the continuum laser source. Since polarization will affect the scattering behavior of the particle [31], the scattering signal would depend on the polarization of the laser source. One way to overcome this problem is to insert polarizers at both incident and scattering channels. This makes sure that the polarization of both the incident light and the scattered light is the same for each measurement.

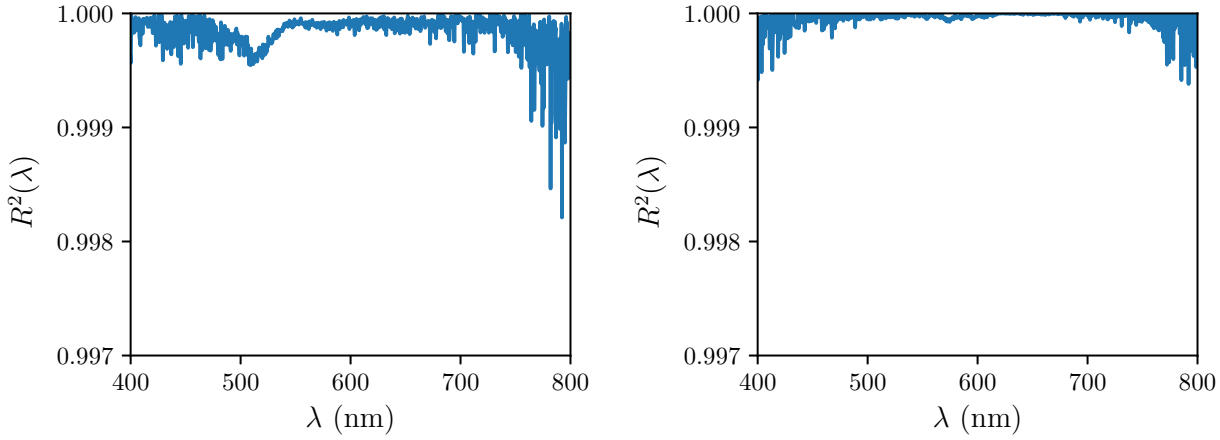

Figure 10: **Coefficient of determination in two analyses:** (a) $R^2(\lambda)$ of the linear fitting for 30 nm Au NPs (b) $R^2(\lambda)$ of the linear fitting for 100 nm Au NPs.

(c) Possible aggregation checking: In section 2.3.2, we checked the linear relation between $P_{out}(\lambda)$ and $C_{r(rel)}$ for 30 nm Au NPs at $\lambda = 541$ nm. Two methods are provided here to confirm that there is no aggregation involved for both 30 nm and 100 nm Au NPs.

1. In statistic, the coefficient of determination, R^2, gives information about the goodness of fit of a model [32]. We calculated $R^2(\lambda)$ for both linear fittings we used in 30 nm and 100 nm Au NPs. As shown in Figure 10, in both cases, $R^2(\lambda)$ are above 0.998. This confirms the linear dependency between the scattering signal and the relative concentrations for both 30 nm and 100 nm Au NPs. Hence, we can assume that our nanoparticles are at single concentration level where no aggregation involves.

2. Instead of fitting a linear function, we calculated $\sigma_{sca}^{p(rel)}(\lambda)$ of 100 nm Au NPs for each $C_{p(rel)}$ directly. The result is shown in Figure 11(a). $\sigma_{sca}^{p(rel)}(\lambda)$ for different concentrations agree well with each other[12]. This high degree of overlap confirms that 100 nm Au NPs are at single particle concentration.

[12]The fluctuation of 1x is due to the low signal to noise ratio.

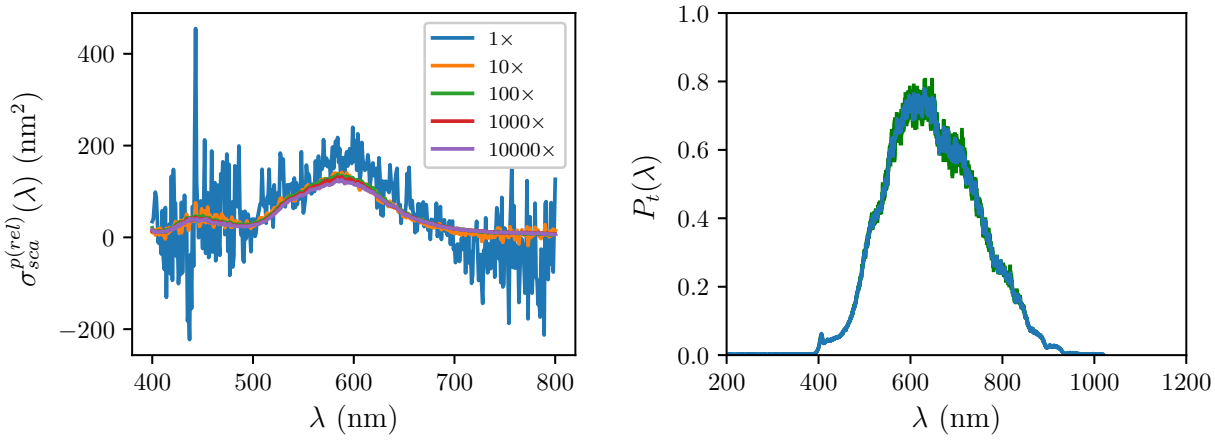

(a) (b)

Figure 11: (a) $\sigma_{sca}^{p(rel)}(\lambda)$ of 100 nm Au NPs for each $C_{p(rel)}$. (b) Transmitted power, $P_t(\lambda)$, was recorded five times. Blue line is their mean value and green line is their standard deviation. The unit of $P_t(\lambda)$ on the vertical axis is Relative Counts / ms.

(d) Fluctuation of the input power: We assumed that $P_{in}(\lambda)$ stays the same in both reference and reliability measurements. Whether this assumption is valid need to be verified by the reproducibility test of our laser. In this reproducibility test, we recorded $P_t(\lambda)$ for five rounds, where each round was measured after the laser was restarted. Mean value and the standard deviation were shown in Figure 11(b). $P_t(\lambda)$ does not fluctuate very much during the measurements. Since $P_t(\lambda)$ scales with $P_{in}(\lambda)$, this reliability measurement confirmed that $P_{in}(\lambda)$ is stable during our measurements.

2.4 Applications

We presented the setup for measuring SCS of small particles. In this section, we implement the same reference (30 nm Au NPs) and experimental scheme to two particles: CPSAA and Rhodamine 6G (R6G). CPSAA is a pH-sensitive nanoparticle. Its size depends on the pH value of the solution. By observing the change of its relative SCS, we analysed the change of its size. The other particle is R6G, a highly fluorescent dye. It emits high elastic scattering signal at certain wavelength, called resonance light scattering (RLS). We measured its scattering signal through our setup.

2.4.1 Size measurements of pH-sensitive particles

(a) Introduction to CPSAA: CPSAA is synthesized by decorating polyacrylic acid (PAA) brush on the surface of polystyrene nanosphere [33]. The thickness of PAA layer depends on the concentration of the hydrogen ion in the solution, as illustrated in Figure 12. Based on coated sphere model in Mie theory [34], change of the coating thickness leads to change of SCS. Hence, the SCS of CPSAA is dependent on the pH of the solution.

By implementing our setup, we observed the pH-sensitive behavior of CPSAA through its

SCS. We simulated this process using coated sphere model in the Mie theory. By adjusting the thickness of the coating, we fitted our theory to the experimental data and extracted the size information of CPSAA.

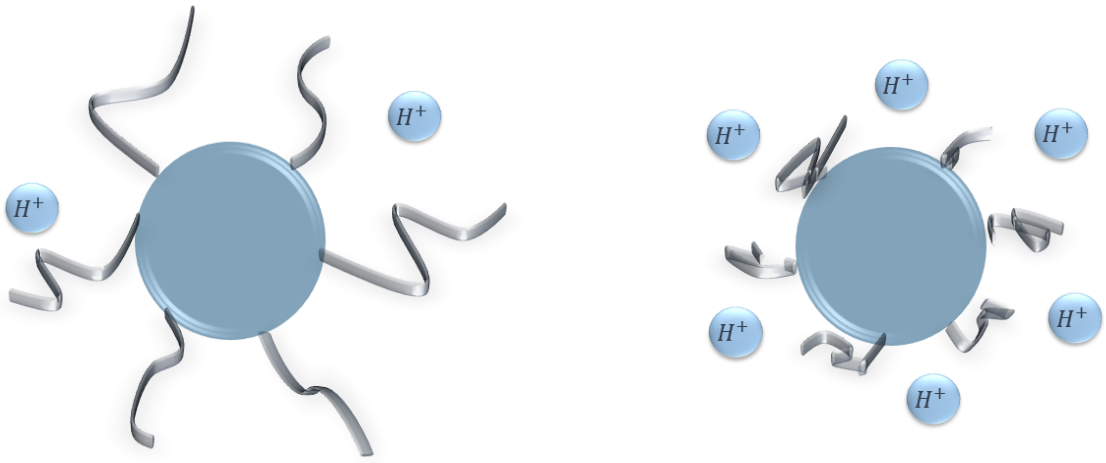

(a) (b)

Figure 12: **Illustration of the pH-sensitive behavior of CPSAA:** (a) CPSAA at high pH environment: brush streches. (b) CPSAA at low pH environment: brush gets suppressed by the hydrion.

(b) Measuring relative SCS of CPSAA: We prepared 8 groups of dilution series of CPSAA[13]. Each group has different pH value, varying from 0 to 7. We obtained relative SCSs σ_{sca}^{rel} of CPSAA for different pH values[14], as shown in Figure 13. From the result, we see that the σ_{sca}^{rel} is dependent on the pH. As shown in Figure 13(a), after pH drops below 2, the relative SCS decreases along the pH. This implies that CPSAA shrinks as pH decreases at this range. In Figure 13(b), we normalized the relative SCSs over their peak values. We only investigated the normalized SCSs[15].

(c) Theoretical Fitting: If we consider CPSAA as a sphere with coating layer, we can simulate its SCS using Mie theory [35]. We fit the theoretical SCS to our experimental result. The fitting parameter is the thickness of the coating. Based on the TEM image of CPSAA shown in Guo Yong's report [33], we set other parameters as follows:

Refractive index of the core	1.59
Refractive index of the coating	1.508
Radius of the core	202 nm

[13]CPSAA was provided by Kegel group, Utrecht University

[14]The procedure of measurement and analysis is the same as section 2.3.3.

[15]We do not analyse the change of relative intensities because we can not justify that the concentration of CPSAA is the same for every pH.

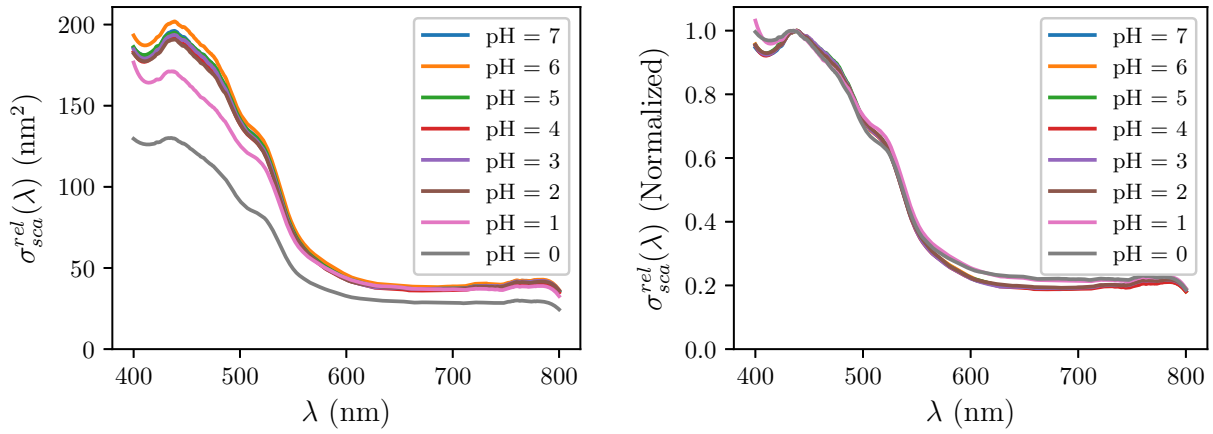

(a) (b)

Figure 13: **Relative SCS σ^{rel}_{sca} of CPSAA in different pH:** (a) σ^{rel}_{sca} of CPSAA in different pH (b) normalized σ^{rel}_{sca} respect to the peak value.

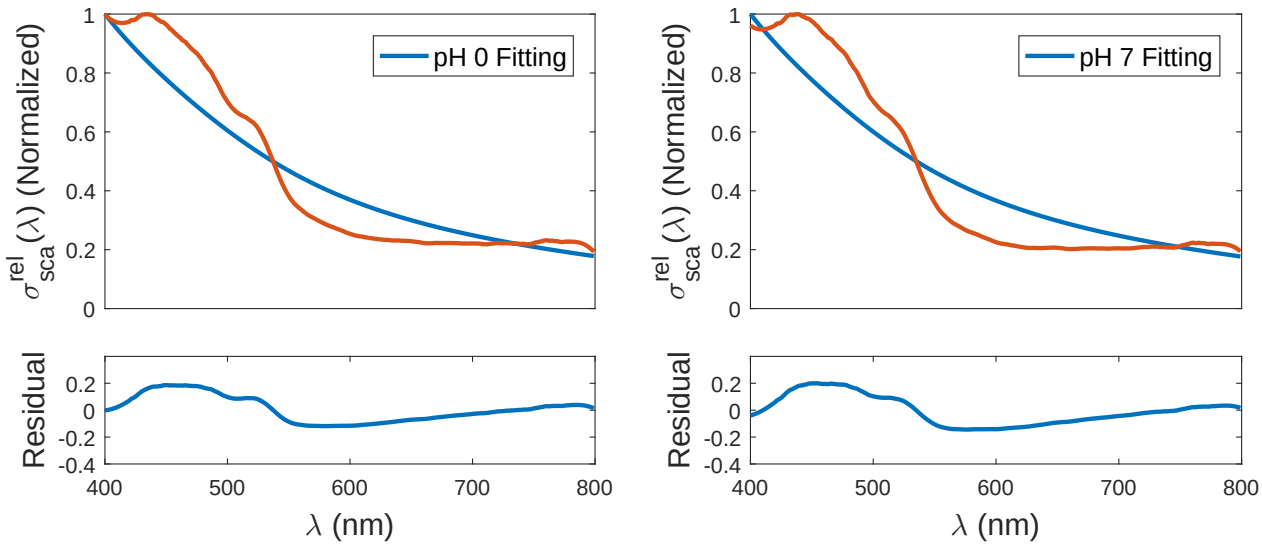

Figure 14: Normalized relative SCS $\sigma^{rel}_{sca}(\lambda)$ and fitting for CPSAA particles at pH 0 and 7. For each fitting, residuals are plotted below. Fitting used Mie coating theory with refractive index of the core as 1.59, refractive index of the brush as 1.508, and radius of the core as 202 nm. Thickness of the coating is used as a fitting parameter which changed from 19.3 nm to 14.9 nm as pH decreased from 7 to 0.

We fitted σ^{rel}_{sca} of CPSAA for pH 0 and 7. The fitting results are shown in Figure 14. From the fitting result, thickness of the coating changes from 19.3 nm to 14.9 nm from pH 7 to pH 0. This agrees with our anticipation that the thickness of the coating decreases when pH becomes smaller.

(d) Conclusion and outlook for CPSAA: By measuring relative SCSs of CPSAA and fitting them to Mie theory, we found out that the thickness of the coating shrunk 5 nm while pH drops from 7 to 0. This shows that we can qualitatively detect small change of the size of CPSAA through the scattering signal, while modulating the pH of the solution.

Since our setup can detects the pH response, it has the potential to become a pH-sensor. This requirs us to calibrate the scattering signal and the pH value. After the calibration, we should be able to measure the pH of solutions by scattering signal. Thus, with the help of CPSAA, our setup has the potential to be used as a pH-sensor.

(e) Uncertainties: Though we observed 5 nm change of the radius through the fitting function, the degree of change is not the same as others. In the report of Guo Yong [33], the change is 15 nm. This might due to several uncertainties stated below:

1. Uncertainty from the reference: As stated in section 2.3, the SCS of the CPSAA particle is highly dependent on the reference. Any uncertainty in the measurement of the reference would be inherited to the SCS of CPSAA.

2. Uncertainty from the fitting function: In the theoretical fitting, only one fitting parameter was used: coating thickness. However, the refractive index of the coating should also change along the process. The more compressed the coating material is on the surface of the core, the larger its refractive index would become. The ignorance of it is another reason for the disagreement between the simulation and experiment.

2.4.2 Resonance light scattering measurements of fluorophores

(a) Introduction to RLS: In 1995, Pasternack proposed the resonance light-scattering (RLS) technique [10], to efficiently characterize self-assemblies or self-aggregations of chromophores with good electronic coupling [36]. Incident wavelengths were specially considered within their absorption envelopes, and high scattering signals were observed. From then on, it has received an increasing attention by analysts, as a consequence exhibiting more and more fascinating analytical applications. Due to its absorbing nature, molecules also exhibit RLS. However, no absolute SCS measurement of single molecules has been conducted.

Motivated by this, we designed our setup to measure the absolute SCS of a single molecule R6G. R6G is a highly fluorescent Rhodamine family dye [37]. It is chosen because of its high photostability.

(b) Measurements on Rhodamine 6G: There are two things that need to be taken into account for measuring the SCS of the dye molecule.

1. Dye molecule fluoresces. In order to measure the SCS of a particular wavelength, the incident light need to be monochromatic to avoid any fluorescent signal caused by other excitation wavelength.

2. Due to the large absorption that dye molecule would cause, there is loss in our scattering signal. This loss highly depends on the concentration of the R6G. Thus, instead of only measuring the scattering signal, we also need to monitor the transmission signal to record the absorption of the light.

We implemented a monochromator in front of our incident channel to solve the first problem. However, though an experimental scheme for particles with large extinction has been developed at section 2.2.1, at this stage, we only measured the scattering signal.

In the measurement, we prepared a dilution series of R6G from 0 nM (contrast group) to 10 μM. For each concentration, we recorded the scattering signal, $P_{out}(\lambda)$, at excitation wavelength, $\lambda_{exc.}$, from 405 nm to 705 nm, with an interval of 20 nm.

(c) Results and Theoretical fitting: For the contrast group, $P_{out}(\lambda)$ is from water molecules and background scattering. For other concentrations, $P_{out}(\lambda)$ is from dye molecules, water molecules, and background scattering. In order to obtain the scattering signal only from the dye molecule, we subtract $P_{out}(\lambda)$ by the scattering signal from the contrast group:

$$P^d_{out}(\lambda) = P_{out}(\lambda) - P^0_{out}(\lambda), \tag{23}$$

where $P^0_{out}(\lambda)$ denotes the scattering signal of the contrast group. $P^d_{out}(\lambda)$ is the scattering signal only from the dye molecules.

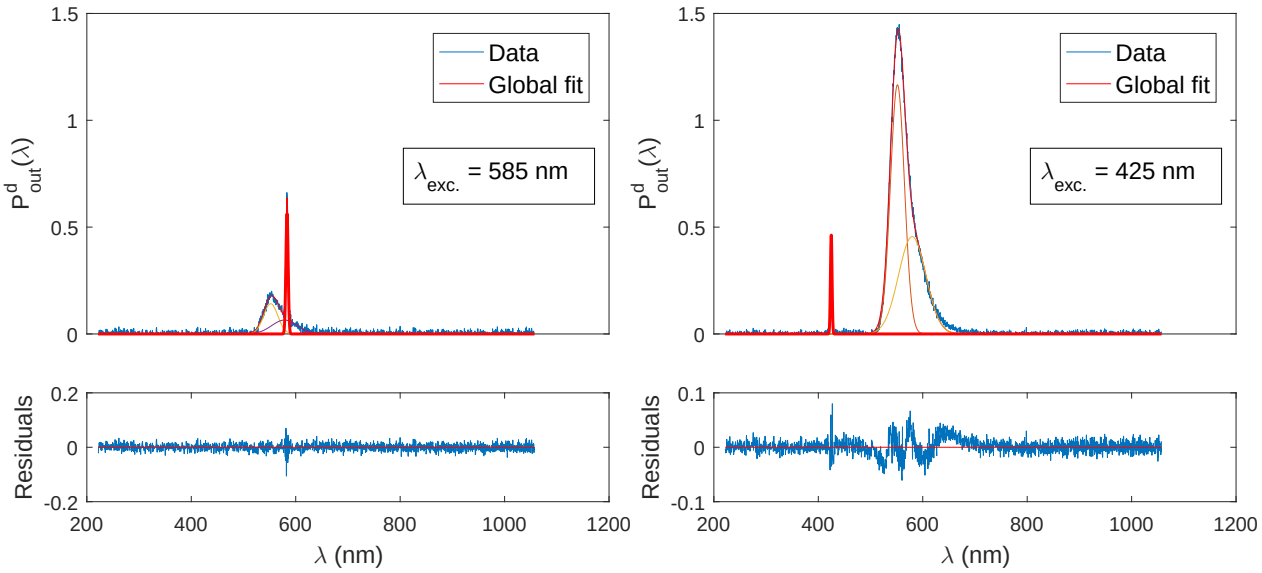

(a) (b)

Figure 15: **Scattering signal from the dye molecules**[16]**,** $P^d_{out}(\lambda)$**, and global fitting for R6G at two excitation wavelength** $\lambda_{exc.}$**:**. Global fitting uses three Gaussian functions to fit $P_{out}(\lambda)$, one for the elastic scattering, the other two for fluorescence (a) $P_{out}(\lambda)$ at $\lambda_{exc.}$ = 585 nm (b) $P_{out}(\lambda)$ at $\lambda_{exc.}$ = 425 nm.

In Figure 15, we present $P^d_{out}(\lambda)$ of 1 μM R6G molecule at $\lambda_{exc.}$ = 585 nm and 425 nm. We used three Gaussian functions to fit $P^d_{out}(\lambda)$. One Gaussian function fits the elastic scattering. The sum of the other two fits the fluorescence. As we can see in Figure 15, the elastic scattering Gaussian at $\lambda_{exc.}$ = 585 nm is higher than the one at $\lambda_{exc.}$ = 425 nm.

[16] $P^d_{out}(\lambda)$ is normalized to the input power, $P_{in}(\lambda_{exc.})$. The relative value of $P_{in}(\lambda_{exc.})$ is measured in appendix B.

(d) Shortcoming: The result shows scattering signals of R6G at two wavelength. However, this is not enough for the absolute SCS measurement. Because the dye molecule has a large absorption, the scattered signal we collected has been attenuated along the light path inside the cuvette, depending on the concentration of the dye molecule. For R6G at 100 nM, the absorption is so strong that $P^d_{out}(\lambda)$ drops below 0 at $\lambda_{exc.} = 605$ nm.

(e) Conclusion and outlook: We measured the RLS of R6G and observed scattering signals at single molecule concentration. However, the absorption of the scattering signal prevents us from measuring its absolute SCS. Further measurement will monitor the transmission signal to offset this absorption.

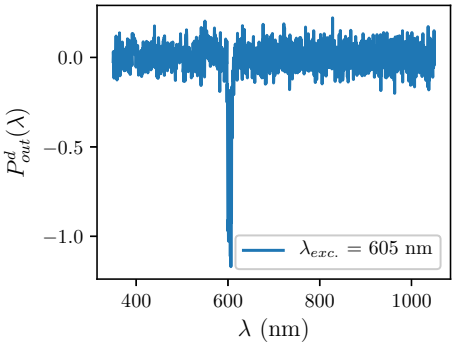

Figure 16: $P^d_{out}(\lambda)$ of 100 nM R6G at excitation wavelength $\lambda_{exc.} = 605$ nm. Unit of $P^d_{out}(\lambda)$ is Relative Counts / ms.

3 Conclusion

In this thesis, we developed a setup for measuring absolute SCS of nanoparticles and single molecules. We tested it using Au NPs. The experimental relative SCSs of Au NPs agree well with theoretical simulations. This confirms the reliability of our setup. We use our setup in two applications. The first application on CPSAA shows that we can detect small change of the size of pH-response particle by measuring its relative SCS. This shows that our setup has the potential to become a pH-sensor. The second application on R6G measured RLS. Elastic scattering signals from fluorophores were observed.

Outlook Currently, we can obtain the relative SCS of nanoparticles with low extinction. In order to measure the absolute SCS of general nanoparticles or single molecules, future improvements need to be made as follows:

1. The size distribution of the reference need to be taken into account. This would provide us a better theoretical SCS of the reference. Thus using this reference, we would get more accurate result when calculating SCSs of other particles.

2. Absolute concentration of Au NPs need to be measured. Since the reason why we couldn't get the absolute SCS is that we do not know the absolute concentration of the Au NPs. Once it's measured, we would be able to calculate the absolute SCS.

3. For the measurement of R6G, we need to monitor the transmission signal to offset the absorption.

Once these problems are solved, we will be able to accurately measure the absolute SCS of nanoparticles or single molecules. The future measurement could lead us towards the absolute SCS of the fluorophores, thus giving a quantitative description of the RLS. The behavior of RLS under the effect of bleaching will also be investigated by our setup.

4 Reference

References

[1] C. F. Bohren and D. R. Huffman, *Absorption and scattering of light by small particles* (John Wiley & Sons, 2008), page 7.

[2] J. W. Strutt, The London, Edinburgh, and Dublin Philosophical Magazine and Journal of Science pp. 107–120 (1871).

[3] A. J. Cox, A. J. DeWeerd, and J. Linden, American Journal of Physics (2002).

[4] S. Weiss, Science (1999).

[5] T. Hirschfeld, Applied optics (1976).

[6] E. B. Shera, N. K. Seitzinger, L. M. Davis, R. A. Keller, and S. A. Soper., Applied optics (1976).

[7] K. Kneipp, Y. Wang, H. Kneipp, L. T. Perelman, I. Itzkan, R. R. Dasari, and M. S. Feld, Physical review letters (1997).

[8] A. Campion and P. Kambhampati, Chemical Society Reviews (1998).

[9] S. Nie and S. R. Emory, Science (1997).

[10] R. F. Pasternack, C. Bustamante, P. J. Collings, A. Giannetto, and E. J. Gibbs., Science **269**, 935 (1995).

[11] J. R. Lackowicz, *Principles of fluorescence spectroscopy* (springer US, 1999).

[12] T. Hirschfeld, Applied optics (1976).

[13] R. I. Ghauharali and G. J. Brakenhoff, Journal of microscopy (2000).

[14] T. Bernas, J. P. Robinson, E. K. Asem, and B. Rajwa, Journal of biomedical optics (2005).

[15] H. P. Lu and S. X. Xie, Nature (1997).

[16] R. M. Dickson, A. B. Cubitt, R. Y. Tsien, and W. E. Moerner, Nature (1997).

[17] H. Lin, S. R. Tabaei, D. Thomsson, O. Mirzov, P.-O. Larsson, and I. G. Scheblykin, Journal of the American Chemical Society (2008).

[18] L. Shaopu and L. Zhongfang, Spectrochimica Acta Part A: Molecular and Biomolecular Spectroscopy (1995).

[19] C. Z. Huang, K. A. Li, and S. Y. Tong, Analytical chemistry (1996).

[20] J. Yguerabide and E. E. Yguerabide, Analytical biochemistry (1998).

[21] J. Yguerabide and E. E. Yguerabide, Journal of Cellular Biochemistry (2001).

[22] Z. Wang, J. Lee, A. R. Cossins, and M. Brust, Analytical chemistry (2005).

[23] C. F. Bohren and D. R. Huffman, *Absorption and scattering of light by small particles* (John Wiley & Sons, 2008), page 477.

[24] C. Mtzler, Tech. Rep. (2002).

[25] P. B. Johnson and R.-W. Christy, Physical review B (1972).

[26] *Nano compposix: Gold nanoparticles*, URL `https://nanocomposix.eu/pages/gold-nanoparticles-optical-properties`.

[27] R. R. Alfano, *The supercontinuum laser source* (1989).

[28] *Instrument response correction*, URL `http://www.horiba.com/fileadmin/uploads/Scientific/Documents/OSD/203_Instrument_Response_Corrections.pdf`.

[29] S. Link and M. A. El-Sayed, Annual review of physical chemistry (2003).

[30] S. Underwood and P. Mulvaney, Langmuir (1994).

[31] C. F. Bohren and D. R. Huffman, *Absorption and scattering of light by small particles* (John Wiley & Sons, 2008), page 62.

[32] *Coefficient of determination definition*, URL `http://stattrek.com/statistics/dictionary.aspx?definition=coefficient_of_determination`.

[33] Y. Guo, B. G. van Ravensteijn, C. H. Evers, and W. K. Kegel, Langmuir (2017).

[34] C. F. Bohren and D. R. Huffman, *Absorption and scattering of light by small particles* (John Wiley & Sons, 2008), page 148.

[35] C. F. Bohren and D. R. Huffman, *Absorption and scattering of light by small particles* (John Wiley & Sons, 2008), page 483.

[36] W. Lu, B. S. F. Band, Y. Yu, Q. G. Li, J. C. Shang, C. Wang, Y. Fang, et al., Microchimica Acta **158**, 29 (2007).

[37] R. F. Kubin and A. N. Fletcher, Journal of Luminescence (1982).

[38] J. D. Jackson, *Electrodynamics* (1975), section 5.18A.

[39] *Acceptance cone*, URL `http://www.timbercon.com/Acceptance-Cone.html`.

[40] *Supercontinuum laser*, URL `http://www.nktphotonics.com/product/sc400-4-compact-supercontinuum-laser/`.

Appendix

A Derivation of the relation between scattering signal and particle concentration

The input power of the broadband laser is $P_{in}(\lambda)$. As illustrated in Figure 17, $L_{in}(\vec{r})$ is the length light travelled from the incident channel to a particle at position, $\vec{r}$. The intensity, $I(\vec{r},\lambda)$, of the incident light at $\vec{r}$ is determined by the transmission factor, $\alpha(\vec{r},\lambda)$, and extinction, $e^{-\frac{L_{in}(\vec{r})}{L_{ext}(\lambda)}}$:

$$I(\vec{r},\lambda) = \alpha(\vec{r},\lambda)P_{in}(\lambda)e^{-\frac{L_{in}(\vec{r})}{L_{ext}(\lambda)}}. \tag{24}$$

The extinction is caused by particles in the solution. $L_{ext}(\lambda)$ is the penetration depth of the solution [38]. The scattered power, $P_{sca}(\vec{r},\lambda)$, of a particle at $\vec{r}$ is

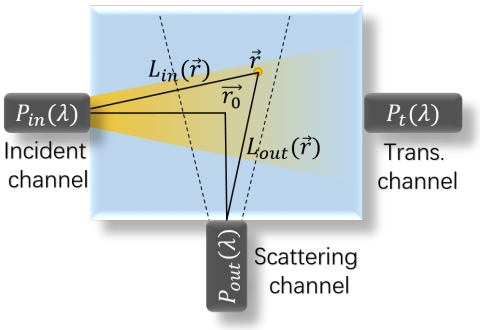

Figure 17: Setup illustration

$$P_{sca}(\vec{r},\lambda) = I(\vec{r},\lambda)\sigma^p_{sca}(\lambda) \tag{25}$$

where σ^p_{sca} is the SCS of a particle. The scattered power $dP_{sca}(\vec{r})$ of an amount of particles with concentration, C_p, in a volume, dV, at $\vec{r}$ is

$$dP_{sca}(\vec{r},\lambda) = I(\vec{r},\lambda)[\sigma^p_{sca}(\lambda)C_p + \sigma^w_{sca}(\lambda)C_w]dV. \tag{26}$$

There is also scattered power from water molecules. σ^w_{sca} is the SCS of a water molecule. C_w is the concentration of water molecules. This will be competitive when C_p is low. Due to transmission factor, $\beta(\vec{r},\lambda)$, and extinction along the length $L_{out}(\vec{r})$, only a portion of the scattering power, $dP_{sca}(\vec{r},\lambda)$, will be collected by the scattering channel. So the total output power, $P_{out}(\lambda)$, is

$$P_{out}(\lambda) = \iiint_V \beta(\vec{r},\lambda)e^{-\frac{L_{out}(\vec{r})}{L_{ext}(\lambda)}}dP_{sca}(\vec{r},\lambda) + P^{sca}_{bg}(\lambda). \tag{27}$$

The integration volume, V, is the intersaction between two acceptance cones [39] of incident and scattering channels. $P^{sca}_{bg}(\lambda)$ is the background signal collected by the scattering channel, caused by strayed light. We assume it is proportional to the input power $P_{in}(\lambda)$ with a factor, $b_{sca}(\lambda)$:

$$P^{sca}_{bg}(\lambda) = b_{sca}(\lambda)P_{in}(\lambda). \tag{28}$$

Combining equations (26), (27), and (28):

$$P_{out}(\lambda) = \iiint_V \beta(\vec{r},\lambda)\alpha(\vec{r},\lambda)e^{-\frac{L_{out}(\vec{r})+L_{in}(\vec{r})}{L_{ext}(\lambda)}}dV[\sigma^p_{sca}(\lambda)C_p + \sigma^w_{sca}(\lambda)C_w]P_{in}(\lambda) + b_{sca}(\lambda)P_{in}(\lambda). \tag{29}$$

It is simplified if we assume V is small enough:

$$P_{out}(\lambda) = \beta(\vec{r_0},\lambda)\alpha(\vec{r_0},\lambda)e^{-\frac{L_{sca}}{L_{ext}(\lambda)}}V[\sigma^p_{sca}(\lambda)C_p + \sigma^w_{sca}(\lambda)C_w]P_{in}(\lambda) + b_{sca}(\lambda)P_{in}(\lambda). \tag{30}$$

$\vec{r_0}$ is position vector denotes the center of the cuvette. Scattering length $L_{sca} = L_{in}(\vec{r_0}) + L_{out}(\vec{r_0})$.

For the transmission channel, $P_{in}(\lambda)$ will be attenuated by the extinction of particles through transmission length, L_{trans}, with transmission factor, $g(\lambda)$:

$$P_t(\lambda) = g(\lambda)e^{-\frac{L_{trans}}{L_{ext}(\lambda)}}P_{in}(\lambda) + b_{trans}(\lambda)P_{in}(\lambda). \tag{31}$$

$b_{trans}(\lambda)P_{in}(\lambda)$ is the background signal collected by the transmission channel. The ratio between $P_{out}(\lambda)$ and $P_t(\lambda)$ is:

$$\frac{P_{out}(\lambda)}{P_t(\lambda)} = \frac{\beta(\lambda)\alpha(\lambda)\sigma^p_{sca}(\lambda)}{g(\lambda)}C_p + \frac{\beta(\lambda)\alpha(\lambda)\sigma^w_{sca}(\lambda)C_w + b_{sca}(\lambda)e^{-\frac{L_{sca}}{L_{ext}(\lambda)}}}{g(\lambda)} \tag{32}$$

To derive equation (32), two assumptions are made:

1. The scattering length is equal to the transmission length: $L_{sca} = L_{trans}$.

2. The background for the transmission is much less than the signal: $b_{trans}(\lambda) \ll g(\lambda)e^{-\frac{L_{trans}}{L_{ext}(\lambda)}}$.

For simplicity, we write the ratio respect to particle concentration:

$$\frac{P_{out}(\lambda)}{P_t(\lambda)} = k_p(\lambda)C_p + b_p(\lambda) \tag{33}$$

The relation between $k_p(\lambda)$ and $\sigma^p_{sca}(\lambda)$ is:

$$k_p(\lambda) = A(\lambda)\sigma^p_{sca}(\lambda) \tag{34}$$

where $A(\lambda) = \frac{\beta(\lambda)\alpha(\lambda)}{g(\lambda)}$.

B Light source, monochromator, cuvette holder and other experimental elements

Light source: High power white light laser. Model number: SC400 supercontinuum laser. Its power density is shown in Figure 18.

Monochromator: Our home-made monochromator has two modes: broadband mode and monochromatic mode. They are shown in Figure 19. Broadband mode allows the broadband light pass through the monochromator. This mode is used for measuring non-fluorescent particles. Monochromatic mode selects one wavelength in the broadband light. This mode is used for measuring fluorescent particles. A prism controller was programed in python to output given wavelength from monochromator. In the monochromator mode, power for each output wavelength is shown in Figure 20.

Cuvette holder: Cuvette holder is made by 3D-printer in our fab-lab. Its used for connecting all the fibers to the corresponding ports, aligning them to the cuvette.

Cuvette: Si-based high precision cuvette, for storing particle solution used in measurements. Only one cuvette is used because different cuvettes have different background and transmission factors. The position of the cuvette should remain the same in all measurements.

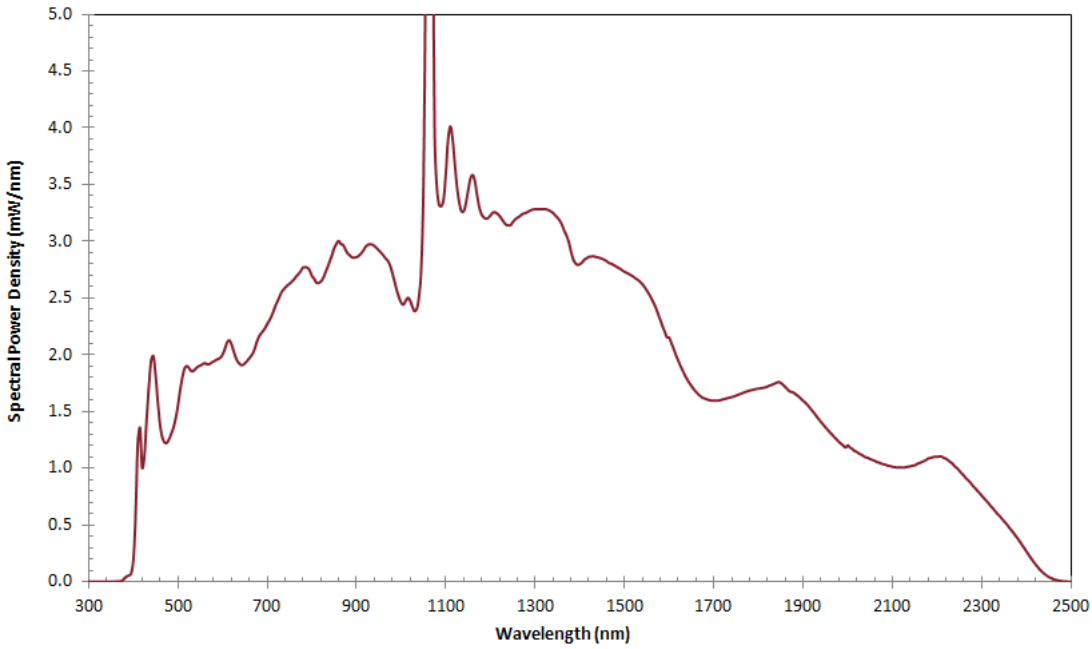

Figure 18: Power density of supercontinuum laser source, from *NKT Photonics* [40].

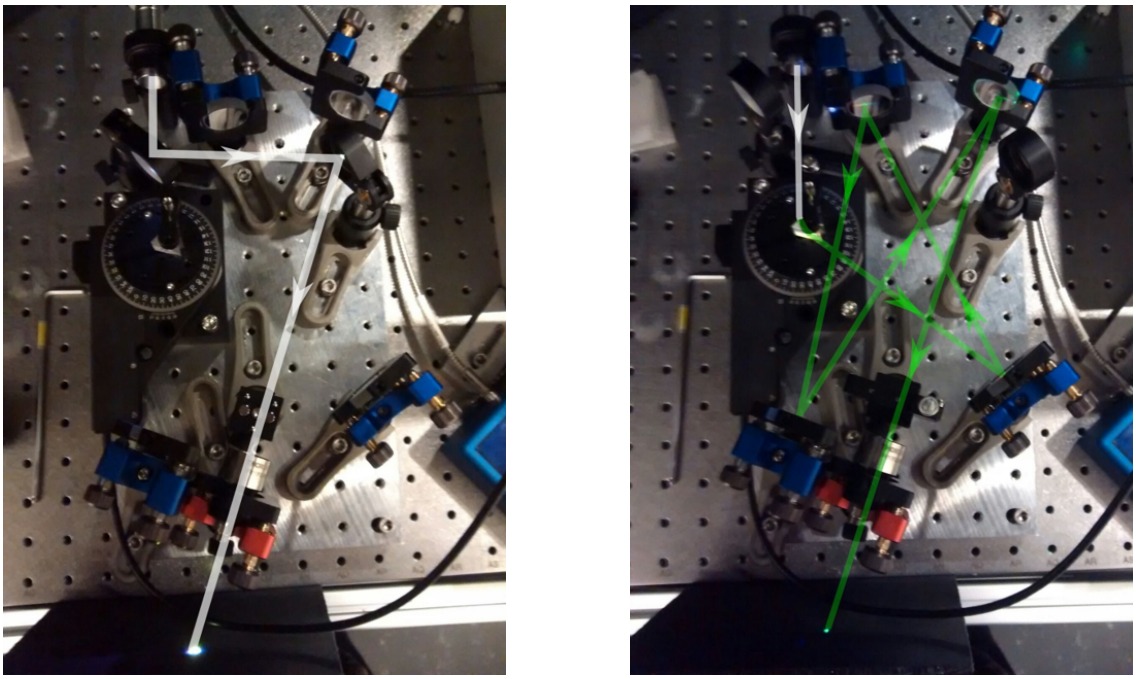

(a) (b)

Figure 19: **Two modes for the monochromator:** (a) broadband mode. Two mirrors are used to reflect the broadband laser to the slit (b) monochromatic mode. The combination of the prism and slit selects one wavelength. Four mirrors are used to increaese the optical distance.

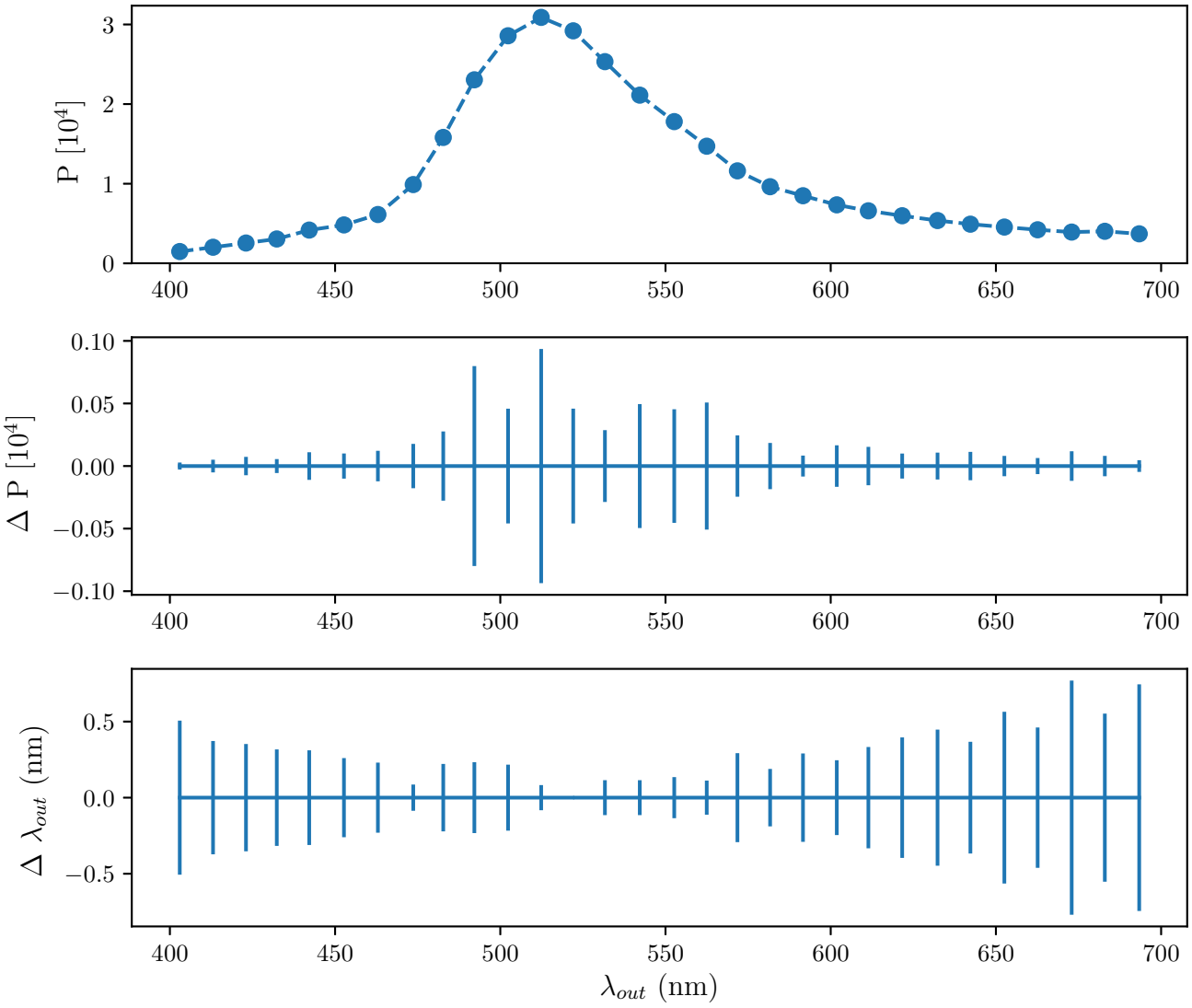

Figure 20: Relative power P for different output wavelength λ_{out}. Standard deviation of the power ΔP and output wavelength $\Delta\lambda_{out}$ are plotted for each output wavelength. The unit of P and ΔP on vertical axises are Relative Counts / ms.